Monthly Notices
of the
ROYAL ASTRONOMICAL SOCIETY

MNRAS **466,** 2325–2336 (2017) doi:10.1093/mnras/stw3139

Statistics of interpulse radio pulsars: the key to solving the alignment/counter-alignment problem

L. I. Arzamasskiy,[1]★ V. S. Beskin[2,3]★ and K. K. Pirov[3]

[1]*Department of Astrophysical Sciences, Peyton Hall, Princeton University, Princeton, NJ 08544, USA*
[2]*P. N. Lebedev Physical Institute, Leninsky prosp., 53, Moscow, 119991, Russia*
[3]*Moscow Institute of Physics and Technology, Dolgoprudny, Institutsky per., 9, Moscow region, 141700, Russia*

Accepted 2016 November 29. Received 2016 November 28; in original form 2016 October 11

ABSTRACT

At present, there are theoretical models of radio pulsar evolution that predict both the alignment, i.e. evolution of inclination angle χ between magnetic and rotational axes to 0°, and its counter-alignment, i.e. evolution to 90°. At the same time, both models describe well the pulsar distribution on the P–$\dot{P}$ diagram. For this reason, up to now it was impossible to determine the braking mechanisms since it was rather difficult to estimate the evolution of the inclination angle based on observations. In this paper, we demonstrate that the statistics of interpulse pulsars can give us the key to solve the alignment/counter-alignment problem as the number of interpulse pulsars (having both $\chi \sim 0^\circ$ and $\chi \sim 90^\circ$) drastically depends on the evolution of the inclination angle.

Key words: stars: neutron – pulsars: general.

1 INTRODUCTION

Almost 50 yr after the discovery of radio pulsars, the problem of the energy loss by neutron stars still remains unsolved (Manchester & Taylor 1977; Smith 1977). In particular, evolution of the inclination angle χ between the magnetic and rotational axes is still unknown. At present, there are theoretical models that predict both the evolution of the inclination angle to 0°, i.e. alignment (Davis & Goldstein 1970; Goldreich 1970; Good & Ng 1985; Philippov, Tchekhovskoy & Li 2014) and its evolution to 90°, i.e. counter-alignment (Beskin, Gurevich & Istomin 1993). Both models are good in describing the P–$\dot{P}$ diagram (which is directly observed), but give completely different answers to the question of the evolution of the inclination angle (for which we have very few observations).

There have been many attempts to resolve the issue by analysing the statistical distribution of radio pulsars (Rankin 1990; Tauris & Manchester 1998; Faucher-Giguère & Kaspi 2006; Weltevrede & Johnston 2008; Young et al. 2010; Gullón et al. 2014). In particular, it was found both directly (i.e. by an analysis of the χ distribution) and indirectly (i.e. from an analysis of the observed pulse width) that statistically the inclination angle χ decreases with period P as the dynamical age $\tau_{\rm D} \approx P/2\dot{P}$ increases. At first glance, these results definitely support an alignment mechanism. However, as was demonstrated by Beskin et al. (1993), the average inclination angle of the pulsar population, $\langle\chi(\tau_{\rm D})\rangle$, computed for observed pulsars, can *decrease* even if the inclination angles of individual pulsars *increases* with time.

Indeed, for given values of the pulsar period P and magnetic field B, secondary pair production over the magnetic polar cap is suppressed at angles χ close to 90°, when the magnetic dipole is nearly orthogonal to the rotational axis. This is because the Goldreich–Julian charge density $\rho_{\rm GJ} \approx \Omega B\cos\chi/(2\pi c)$ is significantly reduced at such angles. This in turn leads to a decrease in the electric potential drop near the surface of the neutron star and suppression of production of secondary particles. Because of the relation between the pulsar extinction line and χ, the average inclination angles of the observed populations can decrease as the dynamical age increases. A detailed analysis carried out by Beskin, Gurevich & Istomin (1984) and Beskin & Eliseeva (2005), based on a kinetic equation describing the distribution of pulsars, provided quantitative proof of this.

Recently, by analysing 45 yr of observational data for the Crab pulsar, Lyne et al. (2013) found that the separation between the main pulse and interpulse increases at the rate of 0.6° per century (implying a similar growth of χ). Even though this supports the counter-alignment model, as was recently shown by Arzamasskiy, Philippov & Tchekhovskoy (2015) and Zanazzi & Lai (2015), the data can be explained with an alignment model as well, if precession with a characteristic time-scale of $\sim$100 yr is considered.

Thus, one can conclude that at present there is no common point of view for the evolution of the inclination angle χ of radio pulsars. On the other hand, it is quite clear that the inclination angle χ is a key hidden parameter and it is impossible to develop a consistent theory of radio pulsar evolution without taking it into account.

★ E-mail: leva@astro.princeton.edu (LIA); beskin@lpi.ru (VSB)

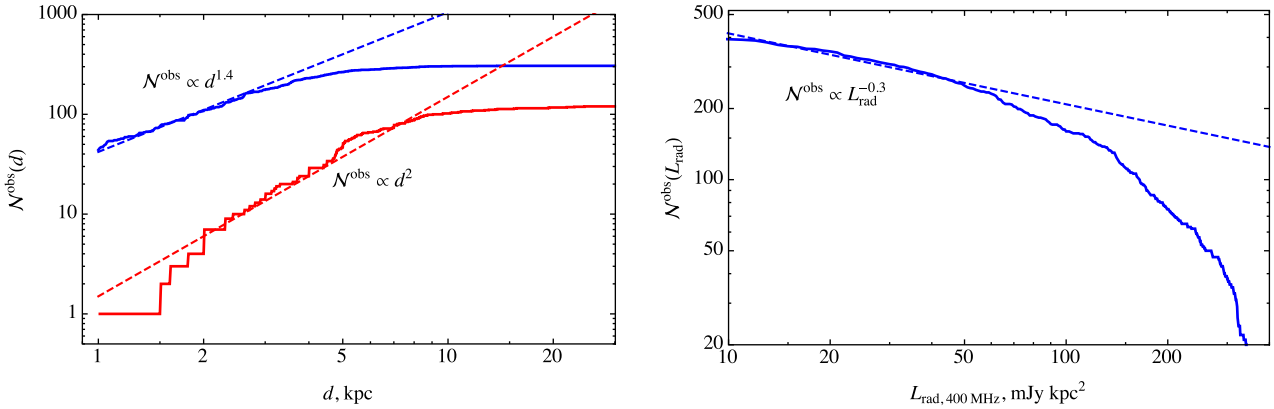

Figure 1. Left: Spatial distribution of radio pulsars $\mathcal{N}^{\rm obs}(d^{\rm obs} < d)$. The upper (blue) curve corresponds to the the main population of pulsars with luminosity $L_{\rm rad} < 400$ mJy kpc^2 measured in the 400-MHz waveband. The lower (red) curve corresponds to the brightest pulsars with radio luminosity $L_{\rm rad} > 400$ mJy kpc^2. The brightest pulsars have distribution function $\mathcal{N}^{\rm obs} \propto d^2$, consistent with homogeneously distributed pulsars in the Galactic disc. However, the main population of pulsars follows a different power law $\mathcal{N}^{\rm obs} \propto d^{1.4}$, which we explain by considering the luminosity distribution function on the right-hand panel. Right: Luminosity distribution function in the 400-MHz waveband $\mathcal{N}^{\rm obs}(L^{\rm obs} > L_{\rm rad})$. At small luminosities, it has an approximate power-law behaviour $\mathcal{N}^{\rm obs} \propto L_{\rm rad}^{-0.3}$, which allows us to explain the behaviour of the pulsar distribution over distances via equation (5).

The aim of this paper is to resolve the alignment/counter-alignment problem by analysing the statistical properties of interpulse pulsars, as the number of such pulsars (both for $\chi \sim 0^\circ$ and $\chi \sim 90^\circ$) mainly depends upon the evolution of the inclination angle.

The paper is organized as follows. Section 2 is an analysis of the observational data, which gives us necessary information about the birth distribution of radio pulsars as well as the visibility function. Here we also give the full list of interpulse pulsars. In Section 3, we discuss two main evolution theories predicting the evolution of alignment and counter-alignment. In Section 4, we describe the details of our population synthesis based on a kinetic equation approach. Finally in Section 5, the main results of our consideration are formulated.

2 RELEVANT OBSERVATIONS

In this section, we gather observational constraints on the pulsar distribution function. Throughout the paper, we use the following notation. We refer to the real distribution function (e.g. the distribution function of *all* pulsars including those which are not observed) over parameter f as $N(f)$. The observed distribution function is different from the real one due to several selection effects. We refer to this function as $N^{\rm obs}(f)$. When describing observations, we often make use of the integrated observed distribution function $\mathcal{N}^{\rm obs}(f) \equiv \int^f N^{\rm obs}(f')\,{\rm d}f'$.

2.1 Spatial distribution

To start with, we need to make some preliminary remarks concerning the general properties of the radio pulsar statistical distribution. It helps us to determine both the visibility function $V^{\rm vis}(P, \chi)$ as well as the birth distribution $Q(P, \chi)$ of radio pulsars. In this section, we analyse the spatial distribution of radio pulsars in the Galactic disc.

Fig. 1 (left-hand panel) shows the observed spatial distribution function of radio pulsars. We divide all pulsars into two groups: the main population (blue, upper curve), which have radio luminosities $L_{\rm rad} < 400$ mJy kpc^2 in the 400-MHz waveband, and the brightest ones, which have $L_{\rm rad} > 400$ mJy kpc^2 (red, lower curve).[1] Only pulsars with known d and $L_{\rm rad}$ are taken into account.

As one can see, the brightest sources show a reasonable integral distribution $\mathcal{N}^{\rm obs}(d) = 2\pi \int_0^d N(d')d'\,{\rm d}d'$:

$$\mathcal{N}^{\rm obs}_{\rm bright}(d) \propto d^{\,2.0} \tag{1}$$

in line with a homogeneous distribution of neutron stars within the Galactic disc. On the other hand, the main population demonstrates a conspicuous deviation:

$$\mathcal{N}^{\rm obs}_{\rm main}(d) \propto d^{\,1.4}. \tag{2}$$

This disagreement can be easily explained if we include the luminosity visibility function $V^{\rm vis}_{\rm lum}$, implying that the receiver with sensitivity S cannot detect distant radio sources with $L_{\rm rad} < 4\pi S d^2$. Indeed, as shown in Fig. 1 (right-hand panel), the visible integral radio luminosity distribution of radio pulsars with $L_{\rm rad} < 400$ mJy kpc^2 has a power-law dependence at small luminosities:

$$\mathcal{N}^{\rm obs}(L_{\rm rad}) \propto L_{\rm rad}^{-0.3}, \tag{3}$$

corresponding to a differential distribution:

$$N^{\rm obs}(L_{\rm rad}) \propto L_{\rm rad}^{-1.3}. \tag{4}$$

By providing a theoretical prediction for the spatial distribution function:

$$\mathcal{N}^{\rm obs}_{\rm th}(d) = 2\pi \int_0^d l\,{\rm d}l \int_{4\pi S l^2}^{\infty} N^{\rm obs}(L_{\rm rad})\,{\rm d}L_{\rm rad} \propto d^{1.4}, \tag{5}$$

we obtain a nice agreement with the observed distribution (2).

Thus, one can conclude that the visible spatial distribution of radio pulsars is compatible with their homogeneous distribution within the Galactic disc. For this reason, below we do not include possible correlations connecting pulsar velocities, their z distribution in the Galactic disc, etc.

[1] Here we use the ATNF pulsar catalogue (http://www.atnf.csiro.au/people/pulsar/psrcat/, Manchester et al. 2005).

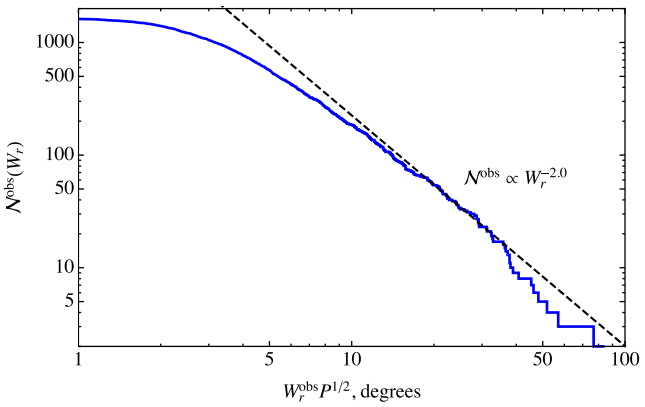

Figure 2. Observed integrated window width distribution $\mathcal{N}^{\rm obs}(W_r) \propto (W_r)^{-2.0\pm0.2}$ determined from statistics of the mean profile width $W_r = W_r^{\rm obs} P^{1/2}$ (taken from the ATNF pulsar catalogue at 50 per cent intensity level). It has an approximate power-law dependence for small inclination angles (large window widths) with index -2, implying that $N^{\rm obs}(\chi) \propto \chi$ at small angles χ.

2.2 Angular distribution

Further, let us try to evaluate the dependence of the distribution of radio pulsars on the inclination angle χ. Unfortunately, as of today, the determination of angle χ by analysing the swing of the linear polarization position angle (Tauris & Manchester 1998; Maciesiak, Gil & Ribeiro 2011; Malov & Nikitina 2013) has some uncertainties, so different authors give different values of the inclination angle. Moreover, the number of pulsars with well-determined inclination angles χ is still rather low (approximately 100–200), thus preventing us from discussing in detail their statistical properties.

For this reason, herein we use the approach proposed by Rankin (1990) and Maciesiak, Gil & Melikidze (2012), which allows us to evaluate the inclination angle for an individual pulsar from the observed width of its mean profile $W_r^{\rm obs}$. Indeed, if W_0 is an intrinsic width of its directivity pattern, then the observed width for $\chi > W_0$ will be equal to

$$W_r^{\rm obs} = \frac{W_0}{\sin\chi}. \tag{6}$$

As was found by Rankin (1990, 1993) and Maciesiak et al. (2012), there are different values of W_0 for the conal and core components of emission. In this paper, we mainly use the value of W_0 corresponding to the conal component (as was also used in Weltevrede & Johnston 2008):

$$W_0 = \frac{5.4^\circ}{\sqrt{P}}. \tag{7}$$

Here, factor $P^{-1/2}$ (where P is in seconds) corresponds to the clear period dependence upon open magnetic field lines, which just determines the diagram width. As a result, relations (6) and (7) allow us to evaluate the angular distribution of radio pulsars on much richer statistics.

As is shown in Fig. 2, the observed window width distribution $\mathcal{N}^{\rm obs} = \int N(W_r)\,{\rm d}W_r$ for $W_r = W_r^{\rm obs} P^{1/2} < 35^\circ$ features a power-law dependence corresponding to differential distribution

$$N^{\rm obs}(W_r) \propto (W_r)^{-3.0}. \tag{8}$$

As

$$N^{\rm obs}(\chi) = N^{\rm obs}(W_r)\frac{{\rm d}W_r}{{\rm d}\chi}, \tag{9}$$

one can conclude that the observed angular distribution $N^{\rm obs}(\chi)$ at small angles is proportional to χ:

$$N^{\rm obs}(\chi) \propto \chi, \tag{10}$$

which is in good agreement with observations (Tauris & Manchester 1998; Maciesiak et al. 2012).

For $\chi > W_0$, the beaming visibility function $V_{\rm beam}^{\rm vis}$ (which takes into account that the observer must be located within the directivity pattern of the radio beam) can be written as $V_{\rm beam}^{\rm vis} = \sin\chi\, W_r^{\rm obs}$. Accordingly, if one can put $N^{\rm obs}(\chi) = V_{\rm beam}^{\rm vis}(\chi) N(\chi)$, the real distribution function $N(\chi)$ for small angles χ is approximately constant:

$$N(\chi) \approx {\rm const} \quad \text{(small angles)}. \tag{11}$$

Thus, we conclude that when analysing the observed distribution of radio pulsars, it is necessary to involve the beaming visibility function $V_{\rm beam}^{\rm vis}$, which in the general case can be approximately formulated as (see a more accurate definition in Section 2.3):

$$V_{\rm beam}^{\rm vis} = \begin{cases} \sin\chi\, W_0, & \chi > W_0, \\ W_0^2, & \chi < W_0. \end{cases} \tag{12}$$

It is interesting that the break for $W_r > 35^\circ$ (see Fig. 2) just corresponds to inclination angles $\chi < W_0$ when the lower expression in (12) is to be used.

2.3 Visibility function

The observed distribution function $N^{\rm obs}$ of radio pulsars deviates from the real distribution function N. That difference comes from two main effects.

The first is because we cannot observe distant faint sources. As we show in Section 2.1, the observed spatial distribution of radio pulsars agrees with a homogeneous distribution. Thus, if $L(P, \chi, B)$ is the pulsar luminosity and S is the receiver sensitivity (radiation is assumed to be isotropic and the anisotropy of the radiation can be accounted for by properly renormalizing function L), one can calculate the impact on the distribution function due to the limited sensitivity:

$$\begin{aligned} N^{\rm obs} &= \int_0^{R_{\rm max}} 2\pi l\,{\rm d}l\, N\Theta\left[S - L/4\pi l^2\right] \\ &= \frac{L(P,\chi,B)}{4S} N(P,\chi,B), \end{aligned} \tag{13}$$

where $\Theta[x]$ is the Heaviside function and $R_{\rm max}$ is the characteristic radius of the Galactic disc. As most of the pulsars are observed far from the edge of the Galactic disc, we assume $R_{\rm max} \to \infty$. One can see that the observed distribution of pulsars is proportional to their intrinsic luminosity. Interestingly, the distribution function does not depend on receiver sensitivity (assuming that it is constant for all pulsars), as this will disappear after normalization.

Unfortunately, the function $L(P, \chi, B)$ is poorly constrained, as the pulsar radio luminosity weakly depends on observed parameters P and $\dot{P}$. A recent review by Bagchi (2013) contains the radio luminosity of most of the proposed models. The dependence of luminosity L on P and $\dot{P}$ is usually expressed as

$$L \propto P^{\alpha_1} \dot{P}^{\alpha_2} \tag{14}$$

with parameters α_1 and α_2 used to fit the data. This expression, although widely used, is only observationally motivated. Up to now, there has been no physically motivated model describing pulsar luminosity in terms of the intrinsic parameters P, χ and B. Early

studies (e.g. Vivekanand & Narayan 1981) tried to find optimal pairs (α_1, α_2) by fitting the observed values of luminosities. Such studies give values $(\alpha_1, \alpha_2) \sim (-0.8, 0.4)$. Later studies (e.g. Faucher-Giguère & Kaspi 2006; Bates et al. 2014) take into account selection effects and include (α_1, α_2) as a part of the population synthesis model. Although in principle it should give more accurate values, it introduces two additional free parameters and makes the synthesis more uncertain. These studies suggest values $(\alpha_1, \alpha_2) \sim (-1.5, 0.5)$.

On the other hand, there are only a few theoretical studies on pulsar radio luminosities. For example, the counter-alignment model (Beskin et al. 1993) predicts

$$L(P, \chi, B) \propto P^{-0.8\pm0.2} \cos^{1/2} \chi, \tag{15}$$

while for the alignment model there is no such prediction. Due to such poor constraints on the luminosity function, in the majority of the paper, we use a simplified version:

$$L(P, \chi, B) = L(P) \propto P^{-1}, \tag{16}$$

implying that we can rewrite the distribution function as

$$N^{\rm obs} = V^{\rm vis}_{\rm lum}(P) N \propto P^{-1} N, \tag{17}$$

where

$$V^{\rm vis}_{\rm lum}(P) \propto P^{-1}. \tag{18}$$

This simplification allows us to express the results in a compact form. However, our analysis is general and can be easily modified for an arbitrary visibility function. We discuss the influence of the luminosity function on pulsar statistics as well as the dependence of L on the inclination angle and magnetic field in Section 4.5.

Another important effect is the beaming of the radio emission. If a pulsar has an inclination angle χ and the angle between its rotational axis and the direction to the observer is ξ, the pulsar can be seen only if

$$|\chi - \xi| < W_0, \tag{19}$$

where both angles should lie between 0° and 90°. It is natural to assume the direction to the observer is randomly distributed, which implies $N(\xi) = \sin\xi$. Then we can determine the beaming visibility function from

$$V^{\rm vis}_{\rm beam} = \int_{\xi_{\rm min}}^{\xi_{\rm max}} \sin\xi \, {\rm d}\xi, \tag{20}$$

where $\xi_{\rm min} = \max(0, \chi - W_0)$ and $\xi_{\rm max} = \min(\pi/2, \chi + W_0)$. This is a general expression, and in the limit of small W_0, it is consistent with expression (12).

It is necessary to mention that one should be careful when using expression (7). This expression was obtained from observations of *orthogonal* radio pulsars (e.g. Rankin 1990), for which inclination angles are known. The same expression cannot be reliably used for arbitrary angles. As the coefficient in (7) implies the radio emission is from the very surface of the neutron star, one can expect it to be larger for arbitrary inclined pulsars.

In addition, the radiation visibility function $V^{\rm vis}_{\rm lum}$ has to take into account the death line, which strongly depends upon the inclination angle (see Beskin, Istomin & Philippov 2013 for more details). Indeed, as was already mentioned in the introduction, for given values of pulsar period P and magnetic field B, the production of particles is suppressed at angles χ close to 90°, where the magnetic dipole moment is nearly orthogonal to the axis of rotation. This in turn leads to a decrease in the electric potential drop near the surface of the neutron star and to suppression of the production of secondary particles. For example, within a Ruderman & Sutherland (1975) type model, one can write the following condition for pair creation (Beskin et al. 1993):

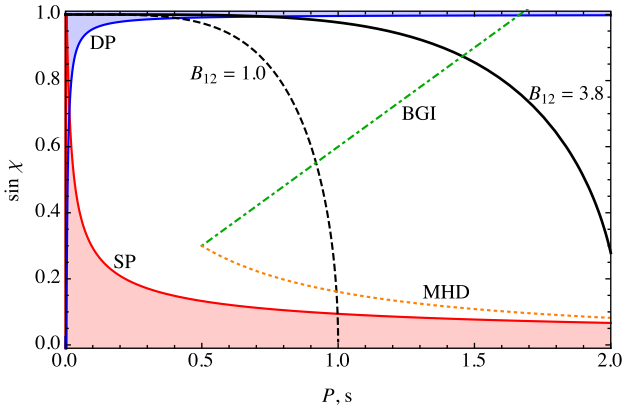

Figure 3. Period–inclination angle diagram. Regions for which it is possible to observe interpulse emission are shaded in blue for double-pole (DP) interpulses, condition (24), and red for single-pole (SP) interpulses, condition (26). Black lines show the pulsar death line (21) for a 10^{12} G magnetic field (dashed line) as well as for a Crab-like pulsar with $B_{12} = 3.8$. The green dot–dashed line shows an example of an evolution curve according to the BGI model, (50) and (51), which is a straight line. The orange dotted line represents the MHD evolution curve according to (44) and (45). The inclination angle of a BGI pulsar increases with time, and it inevitably intersects the death line, leading to a suppression of the number of DP interpulses.

$$\cos\alpha > P^{15/7} B_{12}^{-8/7}, \tag{21}$$

where $B_{12} = B/(10^{12}\,{\rm G})$ and period P is in seconds. Therefore, neutron stars above and to the right of the extinction lines in Fig. 3 cannot be considered as radio pulsars. As will be discussed below, the death line has to be taken into account for orthogonal interpulse pulsars.

2.4 Period distribution

Finally, let us consider the statistical distribution of the period P, which helps us to evaluate the birth function $Q_P(P)$. As is shown on Fig. 4 (left-hand panel), the period distribution function $N^{\rm obs}(P)$ contains millisecond branch and normal radio pulsars with mean period $P \sim 1$ s. As the evolution of millisecond pulsars differs essentially from the evolution of ordinary pulsars (see, e.g., Lyne & Graham-Smith 1998), in what follows we consider the pulsars with $P > 0.03$ s only. At first glance, the distribution of ordinary pulsars is like a log-normal one, as is generally assumed for the birth function (Popov & Prokhorov 2007; Gullón et al. 2014). However, as is shown in Fig. 4 (right-hand panel), in reality, for small P, the distribution function clearly is a power law:

$$N^{\rm obs}(P) \propto P^{0.5} \tag{22}$$

until $P \sim 0.5$ s. In what follows, we consider *only* the pulsars with $0.03\,{\rm s} < P < 0.5\,{\rm s}$, and assume (22) as their observational distribution function.

Using now the total visibility functions (12) and (18), one can conclude that $V^{\rm vis} = V^{\rm vis}_{\rm lum} V^{\rm vis}_{\rm beam} \propto P^{-1.5}$. Hence, the real differential distribution function $N(P)$ for small periods P has the form

$$N(P) \propto P^2. \tag{23}$$

This power law for small periods is enough for us, as the interpulse pulsars have rather small periods $P \sim 0.1$–0.5 s as well (see red

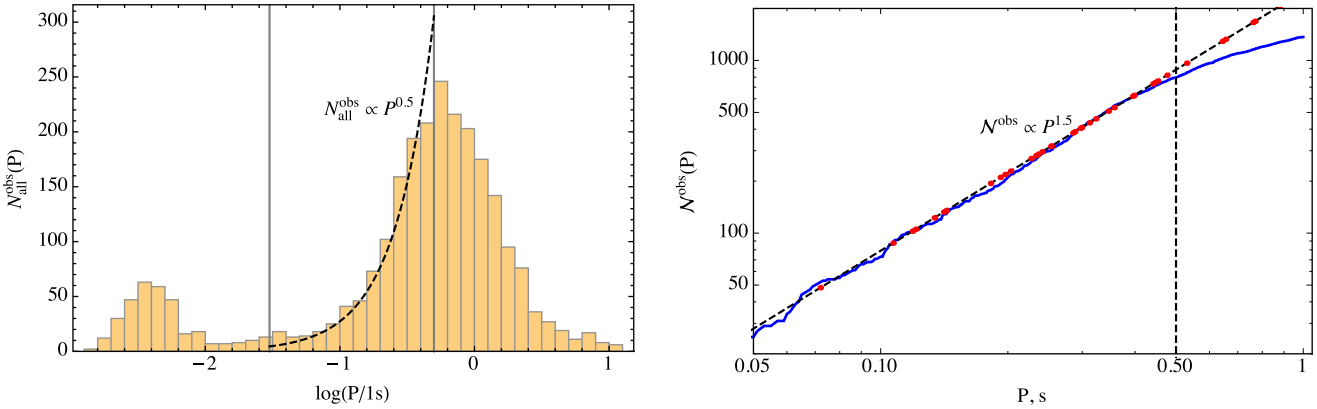

Figure 4. Left: Period distribution function for all pulsars. The bump to the left corresponds to millisecond pulsars, and to the right of it are normal pulsars. In this paper, we consider only pulsars between two vertical lines that have periods $0.03\ {\rm s} \le P \le 0.5\ {\rm s}$. In this period range, the period distribution is approximately a power law $N^{\rm obs} \propto P^{0.5}$. Right: Integral period distribution function $\mathcal{N}^{\rm obs}(P^{\rm obs} < P)$ of normal pulsars. The distribution function is a power law until $P \sim 0.5$ s. Red dots show the locations of pulsars with interpulse emission.

points in Fig. 4). For the same reason, we are not going to take into account the evolution of the magnetic field, as the time-scale of its evolution is larger than the dynamical age of ordinary pulsars $\tau_{\rm D} \approx P/2\dot{P}$.

2.5 Interpulse pulsars

2.5.1 *Single- and double-pole interpulse pulsars*

As was already mentioned, interpulse pulsars can provide an insight on the evolution of radio pulsars because they can provide additional information about the inclination angle χ. Indeed, as is well known (Manchester & Taylor 1977; Lyne & Graham-Smith 1998), the interpulse appears when we observe either two opposite poles (a double-pole or DP pulsar) or the same pole twice (a single-pole or SP pulsar); in the latter case, the two peaks correspond to the double intersection of the hollow-cone directivity pattern. For the DP case, the inclination angle χ is close to 90°, while for a SP pulsar, this angle is close to 0°.

It is necessary to underline that sometimes it is rather difficult to make a clear distinction between SP and DP interpulse pulsars. The determination of the inclination angle from polarization characteristics is kind of blurred, so some additional arguments must be used. For example, one can suppose that for SP pulsars, the main pulse/interpulse separation is not equal to 180° and is frequency dependent, and there is non-zero radio emission between pulses. Accordingly, the angular separation of the two components for DP interpulse pulsars is close to 180° and does not depend on the frequency, and there is no radio emission between them.

2.5.2 *Interpulse statistics*

There are several catalogues of interpulse pulsars. The most full ones were made by Maciesiak et al. (2011) and by Malov & Nikitina (2013). We collect such pulsars in Table 1, which includes the pulsar names, their periods and period derivatives P and $\dot{P}$, interpulse/mean pulse intensity ratio, and angular separation between peaks. In addition, we show the SP/DP classification from Maciesiak et al. (2011) and Malov & Nikitina (2013). As one can see, there is some disagreement in their interpretation resulting from the different approaches in determining the inclination angle from polarimetric properties. In this work, we do not aim at resolving this disagreement.

It is necessary to stress that one of the main features of interpulse pulsars is their rather small periods P compared to the total population, as presented on Fig. 4. Accordingly, their dynamical ages $\tau_{\rm D} \approx P/2\dot{P}$ are much less than those of most radio pulsars (∼1–10 Myr). Besides, as is shown in Table 2, the number of interpulse pulsars in the period range $0.03\ {\rm s} < P < 0.5\ {\rm s}$ is much larger than outside this range $P > 0.5$ s. Thus, by considering this period range and using the distribution function of all pulsars $N^{\rm obs} \propto P^{0.5}$, we can describe most of the interpulse pulsars with good accuracy.

2.5.3 *Visibility function*

For interpulse pulsars, it is necessary to make a correction to the beaming visibility function. For almost orthogonal DP interpulses, the condition to see two oppositely directed poles has the form

$$\pi - \chi - \xi < W_0, \tag{24}$$

which means that the visibility function

$$V_{\rm beam}^{\rm vis,DP} = \int_{\xi_{\rm min}^{\rm DP}}^{\pi/2} \sin\xi {\rm d}\xi, \quad \xi_{\rm min}^{\rm DP} = \min(\pi/2, \pi - W_0 - \chi). \tag{25}$$

For SP interpulses, the condition to see the same pole twice is (Weltevrede & Johnston 2008)

$$\chi + \xi < W_0, \tag{26}$$

implying the visibility function is

$$V_{\rm beam}^{\rm vis,SP} = \int_0^{\xi_{\rm max}^{\rm SP}} \sin\xi {\rm d}\xi, \quad \xi_{\rm max}^{\rm SP} = \max(0, W_0 - \chi). \tag{27}$$

However, equation (26) underestimates the fraction of SP interpulses. Equation (26) implies that the observer can see the emission region over the whole rotation period. However, given that the angular separation between the main pulse and the interpulse for SP interpulses is often less than 180° (see Table 2), we get the following *necessary* condition for an SP interpulse:

$$\xi^2 + \chi^2 - 2\xi\chi\cos\eta \le W_0^2, \tag{28}$$

Table 1. All known interpulse pulsars. [1] from Maciesiak et al. (2011) and [2] from Malov & Nikitina (2013). There is significant disagreement between these studies. We do not aim to resolve this disagreement. Instead, we treat the discrepancy in the classification as the uncertainty in observational constraints (see Table 2).

Name J	P [s]	$\dot{P}$ 10^{-15}	IP/MP ratio	Sep. [°]	[1]/[2]
0534+2200	0.033	423	0.6	145	–/–
0627+0706	0.476	29.9	0.2	180	DP/DP
0826+2637	0.53	1.7	0.005	180	DP/–
0828−3417	1.85	1.0	0.1	180	SP/–
0831−4406	0.312	1.3	0.05	234	SP/SP
0834−4159	0.121	4.4	0.25	171	DP/SP
0842−4851	0.644	9.5	0.14	180	DP/DP
0905−5127	0.346	24.9	0.059	175	DP/–
0908−4913	0.107	15.2	0.24	176	DP/DP
0953+0755	0.253	0.2	0.012	210	SP/SP
1057−5226	0.197	5.8	0.5	205	DP/SP
1107−5907	0.253	0.09	0.2	191	SP/DP
1126−6054	0.203	0.03	0.1	174	DP/DP
1244−6531	1.547	7.2	0.3	145	DP/SP
1302−6350	0.047	2.28	0.75	145	SP/–
1413−6307	0.395	7.434	0.04	170	DP/DP
1424−6438	1.024	0.24	0.12	223	SP/SP
1549−4848	0.288	14.1	0.03	180	DP/DP
1611−5209	0.182	5.2	0.1	177	DP/–
1613−5234	0.655	6.6	0.28	175	DP/–
1627−4706	0.141	1.7	0.13	171	DP/SP
1637−4553	0.119	3.2	0.1	173	DP/DP
1637−4450	0.253	0.58	0.26	256	SP/SP
1705−1906	0.299	4.1	0.15	180	DP/DP
1713−3844	1.600	177.4	0.25	181	DP/–
1722−3712	0.236	10.9	0.15	180	DP/DP
1737−3555	0.398	6.12	0.04	180	DP/SP
1739−2903	0.323	7.9	0.4	180	DP/DP
1806−1920	0.880	0.017	1.0	136	SP/SP
1808−1726	0.241	0.012	0.5	223	SP/SP
1825−0935	0.769	52.3	0.05	185	–/SP
1828−1101	0.072	14.8	0.3	180	DP/–
1842+0358	0.233	0.81	0.23	175	DP/–
1843−0702	0.192	2.1	0.44	180	DP/–
1849+0409	0.761	21.6	0.5	181	DP/–
1851+0418	0.285	1.1	0.2	200	SP/SP
1852−0118	0.452	1.8	0.4	144	SP/SP
1903+0925	0.357	36.9	0.19	240	SP/SP
1913+0832	0.134	4.6	0.6	180	DP/–
1915+1410	0.297	0.05	0.21	186	DP/–
1932+1059	0.227	1.2	0.018	170	DP/SP
1946+1805	0.441	0.02	0.005	175	SP/SP
2032+4127	0.143	20.1	0.18	195	DP/SP
2047+5029	0.446	4.2	0.6	175	DP/–

Table 2. Number of interpulse pulsars. The lower values correspond to a certain classification (the same determination in [1] and [2]) with high enough interpulse-main pulse intensity ratio IP/MP >0.1.

	0.03/0.5 s	>0.5 s
$\mathcal{N}_{\rm SP}$, observed	4/10	2/3
$\mathcal{N}_{\rm DP}$, observed	10/24	3/5

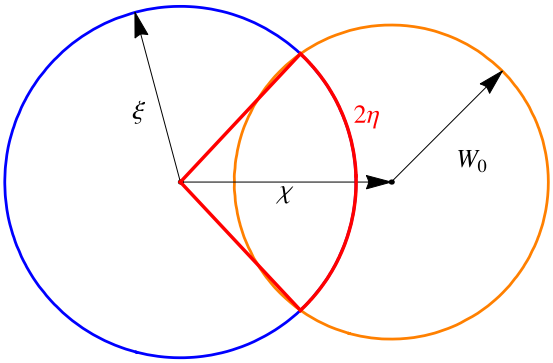

Figure 5. SP interpulse selection criterion. The orange circle represents the boundary of the emission region. In the reference frame rotating with the star, the blue circle corresponds to the trajectory of the line of sight. Since for SP interpulses all angles ξ, χ and W_0 must be small, we can assume that all circles are in the same plane and get the condition (28) for the visible fraction of a period (red) to be larger than 2η.

where η represents the fraction of the period during which the observer can see the emission region (see Fig. 5 for clarification). If $\eta = \eta_{\rm max} = 180^\circ$, equation (28) gives the same constraint as equation (26). However, from Table 1, one can see that the separation between the main pulse and the interpulse for SP pulsars can be as low as 136°, implying $\eta_{\rm min} = 68^\circ$. In what follows, we estimate the number of SP interpulses for both $\eta_{\rm min}$ and $\eta_{\rm max}$, which gives us upper and lower boundaries for interpulse fractions.

It is worth noting that the conditions (27) and (25) do not depend on whether the emission comes from the core or conal component. The geometry of the emission region is parametrized by a single parameter W_0. By changing this parameter, one can consider the core and conal components separately.

3 EVOLUTION THEORIES

3.1 Current losses

As was mentioned above, one of the ways to understand pulsar braking mechanisms is to analyse the evolution of the inclination angle. In the present paper, we consider two magnetospheric theories, both predicting simple analytical expressions for the time evolution of period P and inclination angle χ. The first one is the numerical force-free/magnetohydrodynamics (MHD) model (Spitkovsky 2006; Philippov et al. 2014), which predicts evolution towards 0°. The other one is related to the quasi-analytical model elaborated by Beskin et al. (1984, 1993) and predicts counter-alignment. In both cases, we do not consider the evolution of the magnetic field since most interpulse pulsars have dynamical ages smaller than the characteristic time-scales of magnetic field evolution.

The braking of the neutron star rotation results from the impact of the torque $\mathbf{K}$ due to longitudinal currents $j_\parallel$ circulating in the pulsar magnetosphere; for zero longitudinal current, the magneto-dipole radiation of a star is fully screened by radiation from the pulsar magnetosphere (Beskin, Gurevich & Istomin 1993; Mestel, Panagi & Shibata 1999). General expressions connecting the time evolution of the angular velocity Ω and inclination angle χ can be parametrized as (Beskin et al. 1993; Philippov et al. 2014)

$$I_{\rm r}\dot{\Omega} = K_\parallel \cos\chi + K_\perp \sin\chi \qquad (29)$$

and

$$I_{\rm r}\Omega\,\dot{\chi} = K_{\perp}\cos\chi - K_{\parallel}\sin\chi, \tag{30}$$

where $I_r \propto MR^2$ is the momentum of inertia of the neutron star. We introduce two components of the torque **K**, parallel and perpendicular to the magnetic dipole **m**.

It is convenient to describe these values using the dimensionless current $i \approx j_{\parallel}/j_{\rm GJ}$ by separating it into a symmetric part $i_{\rm s}$ (which has the same sign in the northern and southern parts of the polar cap) and an antisymmetric part $i_{\rm a}$ (which reverses sign on the polar cap). Here and below, we apply normalization to the local Goldreich–Julian current density, $j_{\rm GJ} = |\mathbf{\Omega}\cdot\mathbf{B}|/2\pi$ (with scalar product). For a dipole magnetic field and small angles $\theta - \chi \sim (\Omega R/c)^{1/2}$, we have

$$j_{\rm GJ}(r_m,\varphi_m) \approx \frac{\Omega B_0}{2\pi}\left(\cos\chi + \frac{3}{2}\frac{r_m\sin\varphi_m}{R}\sin\chi\right). \tag{31}$$

Here B_0 is the magnetic field at the neutron star magnetic pole, R is the neutron star radius, and r_m and φ_m are the polar coordinates at the magnetic polar cap. As a result, one can write

$$i_{\rm s} = i_{\rm s}^A\cos\chi \tag{32}$$

and

$$i_{\rm a} = i_{\rm a}^A\sin\chi, \tag{33}$$

where the amplitude values

$$i_{\rm s}^A = \frac{2(I_+ + I_-)}{\Omega B_0 R_0^2\cos\chi} \tag{34}$$

and

$$i_{\rm a}^A = \frac{\pi R(I_+ - I_-)}{\Omega B_0 R_0^3\sin\chi} \tag{35}$$

can be determined by the currents through the northern and southern parts of the polar cap:

$$I_+ = \int_0^{R_0}\int_0^{\pi} j_{\parallel} r_m {\rm d}r_m {\rm d}\varphi_m \tag{36}$$

and

$$I_- = \int_0^{R_0}\int_{\pi}^{2\pi} j_{\parallel} r_m {\rm d}r_m {\rm d}\varphi_m. \tag{37}$$

Here $R_0 \approx (\Omega R/c)^{1/2}R$ is the polar cap radius. For $j_{\parallel} = j_{\rm GJ}$, we have $i_{\rm s}^A = i_{\rm a}^A = 1$.

As one can easily check, $K_{\parallel} \propto i_{\rm s}$ and $K_{\perp} \propto i_{\rm a}$. In particular, the direct action of the Ampère force on the star by surface currents (which are close to the longitudinal electric currents circulating in the pulsar magnetosphere) can be written as (Beskin et al. 1984)

$$K_{\parallel}^{\rm sur} = -c_{\parallel}\frac{B_0^2\Omega^3R^6}{c^3}i_{\rm s} \tag{38}$$

and

$$K_{\perp}^{\rm sur} = -c_{\perp}\frac{B_0^2\Omega^3R^6}{c^3}\left(\frac{\Omega R}{c}\right)i_{\rm a}. \tag{39}$$

Here the coefficients $c_{\parallel}$ and $c_{\perp}$ are factors of order unity that depend on the profile of the longitudinal current and polar cap form. As we see, for a local Goldreich–Julian current $i_{\rm s} \approx i_{\rm a} \approx 1$, relations (38) and (39) imply that

$$K_{\perp}^{\rm sur} \approx \left(\frac{\Omega R}{c}\right)K_{\parallel}^{\rm sur}, \tag{40}$$

so that $K_{\perp}^{\rm sur} \ll K_{\parallel}^{\rm sur}$. Below we also assume (as was not done up to now) that the additional contribution for $K_{\perp}$ can give the magnetosphere itself, more precisely, the mismatch between the magneto-dipole radiation from the magnetized star and radiation from the magnetosphere (which exactly compensate each other for a zero longitudinal current). Here we write down $K_{\perp}^{\rm mag}$ in general form as

$$K_{\perp}^{\rm mag} = -A\,\frac{B_0^2\Omega^3R^6}{c^3}\,i_{\rm a}. \tag{41}$$

We will try to evaluate the dimensionless constant A later from the results of numerical simulations.

Introducing now amplitude values $K_{\parallel}^A = K_{\parallel}(0)$ and $K_{\perp}^A = K_{\perp}(\pi/2)$, we finally obtain

$$I_{\rm r}\dot{\Omega} = K_{\parallel}^A + (K_{\perp}^A - K_{\parallel}^A)\sin^2\chi \tag{42}$$

and

$$I_{\rm r}\Omega\dot{\chi} = (K_{\perp}^A - K_{\parallel}^A)\sin\chi\cos\chi. \tag{43}$$

As both expressions contain the same factor $(K_{\perp}^A - K_{\parallel}^A)$, one can conclude that the sign of $\dot{\chi}$ is associated with a χ dependence of the energy losses (Beskin et al. 2013). In other words, the inclination angle χ evolves towards 90° (counter-alignment) if the total energy losses decrease with increasing inclination angle, and towards 0° (alignment) if they increase with the inclination angle.

3.2 Two braking models

3.2.1 Force-free/MHD model (alignment)

According to the force-free/MHD model based on recent numerical simulations (Philippov et al. 2014), rotation braking and the evolution of the inclination angle can be approximately defined as

$$\dot{\Omega} \approx -\frac{1}{4}\frac{B_0^2R^6\Omega^3}{I_rc^3}(1+\sin^2\chi) \tag{44}$$

and

$$\dot{\chi} \approx -\frac{1}{4}\frac{B_0^2R^6\Omega^2}{I_rc^3}\sin\chi\cos\chi. \tag{45}$$

Accordingly, the total magnetospheric losses are

$$W_{\rm tot}^{\rm MHD} \approx \frac{1}{4}\frac{B_0^2\Omega^4R^6}{c^3}(1+\sin^2\chi), \tag{46}$$

i.e. they increase with the inclination angle χ. The evolution law, (44) and (45), has an integral of motion

$$I^{\rm MHD} = \frac{P\sin\chi}{\cos^2\chi}, \tag{47}$$

which will be used in what follows. As we see, in this model the inclination angle χ evolves to 0°.

It is necessary to point out that, according to equation (40), this case can be realized either for a strong enough anti-symmetric current $i_{\rm a}^{\rm A} \sim (\Omega R/c)^{-1}$, or for a large enough contribution of the magnetospheric torque (41). However, as one can easily find by analysing the analytical asymptotic behaviour of quasi-radial MHD flows (see, e.g. Tchekhovskoy, Philippov & Spitkovsky 2016), the MHD solution (46) corresponds to insufficient value $i_{\rm a}^{\rm A} \sim (\Omega R/c)^{-1/2}$. Remembering that the dimensionless current $i_{\rm a}$ was normalized to the local Goldreich–Julian current $j_{\rm GJ}^{\rm loc}$, we see that the total current circulating in the magnetosphere of the orthogonal rotator is like the axisymmetric case (Bai & Spitkovsky 2010). This is not surprising, because just this total electric current is necessary

for the toroidal magnetic field on the light cylinder to coincide with the electric one. This antisymmetric current for ordinary pulsars with $P \sim 1$ s is 10^2 times larger than the local Goldreich–Julian current. The possibility for the longitudinal current to be much larger than the Goldreich–Julian one was recently discussed by Timokhin & Arons (2013).

Thus, one can conclude that to explain MHD energy losses, it is necessary to suppose the existence of magnetospheric losses with

$$A \approx 2\left(\frac{\Omega R}{c}\right)^{1/2}. \tag{48}$$

Resulting from large enough anti-symmetric currents $i_a \gg 1$, this gives the necessary contribution to total energy losses.

3.2.2 BGI model (counter-alignment)

The analytical theory of pulsar magnetosphere formulated by Beskin et al. (1984, 1993) is based on three key assumptions:

(i) The longitudinal current j_s circulating in the pulsar magnetosphere does not exceed the local one $j_{GJ} \approx \Omega B_0 \cos\chi/2\pi$. Its value is determined by the potential drop in the inner gap V:

$$i_s^A \approx \frac{1}{2}\left(\frac{V}{V_{max}}\right)^{1/2}, \tag{49}$$

where $V_{max} = (\Omega R/c)^2 R B_0$ is the maximum potential drop.

(ii) The potential drop V is determined by the Ruderman & Sutherland (1975) model.

(iii) The magnetospheric contribution $K_\perp^{mag}$ (41) was neglected. As now becomes clear from (41) and (48), this assumption is indeed correct for a small anti-symmetric longitudinal current $i_a \sim 1$, which was also postulated.

As a result, this model provides the following evolution law for $\cos\chi > (\Omega R/c)^{-1}$:

$$\dot{P}_{-15} = Q_{BGI}\frac{B_{12}^2}{P}\cos^2\chi \tag{50}$$

and

$$\dot{\chi} = Q_{BGI}\frac{B_{12}^2}{P}\sin\chi\cos\chi, \tag{51}$$

where again $B_{12} = B_0/(10^{12}\,\mathrm{G})$ and $\dot{P}_{-15} = \dot{P}/10^{-15}$ are the normalized magnetic field and the period derivative, respectively, and P is given in seconds. The main dimensionless parameter of this theory $Q_{BGI} \approx j/j_{GJ}$, for $Q_{BGI} < 1$, can be defined as (Beskin et al. 1984)

$$Q_{BGI} = P^{15/14} B_{12}^{-4/7} \cos^{2d-2}\chi, \tag{52}$$

where $d \approx 0.75$. For $Q_{BGI} > 1$, one has to put $Q_{BGI} = 1$.

As a result, for $\chi \neq 90^\circ$, the Euler equation predicts conservation of the following invariant:

$$I^{BGI} = \frac{P}{\sin\chi}. \tag{53}$$

Thus, within this model, the polar angle χ will increase with time. Accordingly, the total energy losses decrease with an increase of the inclination angle χ:

$$W_{tot}^{(BGI)} \approx i_s^A \frac{B_0^2\Omega^4 R^6}{c^3}\cos^2\chi. \tag{54}$$

Finally, for $Q_{BGI} < 1$, the radio luminosity L can be presented as $L = \alpha W_{part}$, where $W_{part} = Q_{BGI}^2 W_{tot}$ is the particle energy flux and $\alpha \sim 10^{-6}$ is the transformation coefficient. This gives

$$L^{BGI} \propto P^{-0.8}\cos^{1/2}\chi. \tag{55}$$

For $\cos\chi \sim 1$, we return to the evaluation, such as equation (18).

4 PREDICTIONS VERSUS OBSERVATIONS

4.1 General assumptions

4.1.1 Preliminary remarks

To clarify the mechanism of radio pulsar braking, we determine the number of radio pulsars having such angles χ that they can be observed as interpulse pulsars. As their period distribution depends directly on their evolution, this gives us the possibility of recognizing the direction of the evolution of the inclination angle as well. For this reason, we consider the pulsars with $0.03\ \mathrm{s} < P < 0.5$ s for two evolutionary scenarios, (44) and (45), and (50) and (51), using the kinetic equation method. There are two important points to be mentioned.

First, without regard for the smallness of the period P, for interpulse pulsars, the death line will be considered for the orthogonal case for the BGI model. As shown on Fig. 3, for inclination angles χ close to 90°, the death line on the P–sin χ diagram is located at small enough periods $P < 1$ s. Moreover, in this case, the shape of the region within the polar cap where most of the radio emission is produced is not well understood.

Indeed, it is impossible to create pairs near the line where the Goldreich–Julian charge density changes sign, preventing the longitudinal electric field from being large enough. As a result, the geometrical visibility function V_{beam}^{vis} cannot be determined with sufficient accuracy.

On the other hand, numerical kinetic simulations of nearly MHD magnetospheres (Philippov, Spitkovsky & Cerutti 2015) show abundant pair production for large inclination angles. Therefore, for the BGI model, we consider only SP interpulses for which the death line cannot play an important role, while for the MHD model we consider DP interpulses as well.

Secondly, we assume that in the pulsar birth function $Q(P, \chi, B, \xi)$, all arguments are independent of each other:

$$Q(P, \chi, B, \xi) = Q_P(P)Q_\chi(\chi)Q_B(B)\sin\xi. \tag{56}$$

As we already stressed, evolution of the magnetic field is not important for short dynamical ages. This allows us to obtain an exact solution of the kinetic equation with a period distribution that does not depend on the magnetic field birth function.

4.1.2 Initial periods and inclination angles

As was already stressed, the visible distribution of radio pulsars strongly depends on their initial periods P and inclination angles χ. Repeated attempts have been made to determine the birth function $Q_P(P)$ (Lyne, Manchester & Taylor 1985; Popov & Turolla 2012), but so far, this function remains unknown. The new point of our paper is that we use here the direct observational scaling $N^{obs}(P) \propto P^{0.5}$ shown on Fig. 4. Being valid for short periods $P < 0.5$ s, this distribution can describe interpulse pulsars with a high enough precision.

For the birth function Q_χ describing the distribution on initial inclination angles χ, we consider two possibilities, namely $Q_\chi = \sin\chi$ and $Q_\chi = 2/\pi$. The first corresponds to the random orientation of the magnetic axis with respect to the rotational one, which is more reasonable at first glance. However, as we will see, the observational evaluation of the real χ distribution $N(\chi)$ (equation 11) can correspond to the homogeneous distribution $Q_\chi = 2/\pi$ as well.

4.1.3 Comparison with observations

To compare the predictions of evolutionary scenarios with observations, it is not sufficient to know the distribution function of radio pulsars $N(P,\,\chi)$ because it is necessary to consider the visibility functions $V^{\rm vis}$ (see Section 2.1). In particular, the visible distribution of SP interpulse pulsars must be written as

$$N^{\rm obs}(P) = \int_0^{W_r(P)} {\rm d}\chi\, V^{\rm vis}(P,\,\chi)\, N(P,\,\chi). \tag{57}$$

Relation (57) helps us to normalize the observed distribution function as well. We normalize the distribution function by the total number of observed pulsars in the period range 0.03 s $< P <$ 0.5 s:

$$\mathcal{N}_{\rm tot} = \int_{0.03}^{0.5} {\rm d}P \int_0^{\pi/2} {\rm d}\chi\, V^{\rm vis}(P,\,\chi)\, N(P,\,\chi). \tag{58}$$

Observationally, we know that $\mathcal{N}_{\rm tot} = 796$, and in what follows, we use this number to normalize the distribution function.

4.2 Population synthesis: kinetic equation

In this section, we describe our approach using the kinetic equation

$$\frac{\partial}{\partial P}(\dot{P}N) + \frac{\partial}{\partial \chi}(\dot{\chi}N) = Q \tag{59}$$

to obtain the real distribution function $N(P,\,\chi)$ of radio pulsars. Here the values $\dot{P}(P,\,\chi)$ and $\dot{\chi}(P,\,\chi)$ are to be taken from the given model. Accordingly, $Q(P,\,\chi)$ is the birth function depending both on the inclination angle χ and initial period P. Here for simplicity, we put $Q(P,\,\chi) = Q_P(P)Q_\chi(\chi)$. Certainly, we also assumed that the observable distribution is time-independent due to the very small dynamical lifetime $\tau_{\rm D} \approx P/2\dot{P} \sim 10$ Myr in comparison with the Galactic age. Finally, we do not consider magnetic fields in this section, and discuss their impact in Section 4.3.

Due to the existence of integrals of motion, the kinetic equation can be easily solved. Then, adding the visibility functions $V^{\rm vis} = V^{\rm vis}_{\rm lum} V^{\rm vis}_{\rm beam}$ discussed in Section 2.3, one can determine the number of observed pulsars and compare it with observations.

As a result, for the force-free/MHD model (44) and (45), the kinetic equation has the form

$$\frac{\partial}{\partial P}\left[\frac{N}{P}(1+\sin^2\chi)\right] - \frac{\partial}{\partial \chi}\left[\frac{N}{P^2}\sin\chi\cos\chi\right] = K\,Q, \tag{60}$$

where $K = I_r c^3/(\pi^2 B^2 R^6)$. In what follows, we neglect this factor as it disappears after normalization (see also Section 4.3). Using now expression (47) for the integral of motion $I^{\rm MHD}$, we obtain a solution that is valid for arbitrary Q_P and Q_χ:

$$N^{\rm MHD} = \frac{P^2}{\cos^3\chi}\int_\chi^{\pi/2} \frac{\cos^2 x}{\sin x}\, Q_\chi(x) Q_P\left(P\frac{\sin\chi}{\cos^2\chi}\frac{\cos^2 x}{\sin x}\right){\rm d}x. \tag{61}$$

Note that one needs to normalize this solution according to (58). Assuming $N(P) \propto P^2$ (equation 23), one can obtain the birth function $Q_P = {\rm const}$. As a result, for $Q_\chi = 2/\pi$, the solution has a simple form:

$$N^{\rm MHD}(P,\,\chi) = -\frac{2\log\tan(\chi/2) + 2\cos\chi}{\cos^3\chi}\,P^2. \tag{62}$$

Accordingly, for $Q_\chi = \sin\chi$ we have

$$N^{\rm MHD}(P,\,\chi) = \frac{\pi/2 - \chi - \sin\chi\cos\chi}{\cos^3\chi}\,P^2. \tag{63}$$

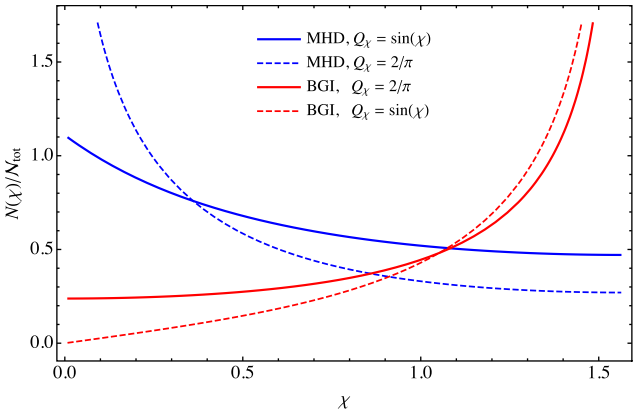

Figure 6. Comparison of angular distribution functions $N(\chi)$ for different evolution models (equations 62, 63, 66 and 67). Models described with dashed lines do not have a finite value in the limit of $\chi \to 0$, and, thus, contradict the observations. On the other hand, models described with solid lines agree with observations. This shows that the MHD and BGI models require different birth function Q_χ to be consistent with observations.

As for the BGI model (50) and (51), the kinetic equation has the form:

$$\frac{\partial}{\partial P}\left[N\cos^{2d}\chi\right] + \frac{\partial}{\partial\chi}\left[\frac{N}{P}\sin\chi\cos^{2d-1}\chi\right] = Q_P(P)Q_\chi(\chi). \tag{64}$$

Using again the integral of motion $I^{\rm BGI}$ (equation 53), we obtain

$$N^{\rm BGI}(P,\,\chi) = \frac{P}{\sin^2\chi\cos^{2d-1}\chi}\int_0^\chi Q_\chi(x)Q_P\left(P\frac{\sin x}{\sin\chi}\right)\sin x{\rm d}x, \tag{65}$$

which again should be properly normalized. As $N(P) \propto P^2$, one can conclude that $Q_P(p)$ is a linear function of p. As a result, for homogeneous angular birth function $Q_\chi = 2/\pi$, the solution looks like

$$N^{\rm BGI}(P,\,\chi) = \frac{\chi - \sin\chi\cos\chi}{\sin^3\chi\cos^{2d-1}\chi}\,P^2. \tag{66}$$

Accordingly, applying the random angular birth function $Q_\chi = \sin\chi$, we obtain

$$N^{\rm BGI}(P,\,\chi) = \frac{2 + \cos^3\chi - 3\cos\chi}{\sin^3\chi\cos^{2d-1}\chi}\,P^2. \tag{67}$$

We present angular distribution functions for different models in Fig. 6. One can easily notice that for the MHD model with a uniform angular birth function (blue dashed line), the number of pulsars with small angles is very large, while for the BGI model and a sinusoidal angular distribution function (red dashed line), the fraction of pulsars with small angles is close to zero. However, observationally one has $N(\chi) \approx$ const at small angles. This implies that the models described with dashed lines in Fig. 6 are inaccurate. On the other hand, models described with solid lines have a finite limit at $\chi \to 0$, and, thus, agree with observations. One should also remember that these distribution functions should be corrected with the visibility function to obtain the observed distribution function.

4.3 Dependence on the magnetic fields

One can immediately see from equation (59) that

$$N \propto Q_\xi(\xi)Q_B(B)\,B^{-2} \quad \text{(MHD)} \tag{68}$$

and

$$N \propto Q_{\xi}(\xi) Q_B(B)\, B^{-10/7} \quad \text{(BGI)}. \tag{69}$$

The observed distribution function $N^{\rm obs}(P, \chi)$ does not depend on the form of the birth function $Q_B(B)$. To show that, we consider the MHD case only, but the same conclusion remains true for the BGI model as well since the only difference is in the power of B in the denominator of equations (68) and (69). The observed distribution function $N^{\rm obs}(P, \chi)$ is given by

$$N^{\rm obs}(P, \chi) = \int_0^{\infty} {\rm d}B \int_0^{\pi/2} {\rm d}\xi\, V_{\rm vis}(P, \chi, B, \xi) N(P, \chi, B, \xi)$$
$$\propto \int_0^{\infty} {\rm d}B\, V_{\rm lum}^{\rm vis}(P, \chi, B) Q_B(B)/B^2. \tag{70}$$

Then, assuming $V_{\rm lum}^{\rm vis} \propto \dot{P}^{\alpha_2} \propto B^{2\alpha_2}$, we get $N^{\rm obs} \propto \int {\rm d}B B^{2\alpha_2 - 2} Q_B(B)$. So, the dependence of the source function on the magnetic field gets factored out. The assumptions allow us to find a solution that does not depend on the initial magnetic fields.

Of course, the main assumption here is that the luminosity visibility function has a specific form. This assumption is widely used in the literature (Bagchi 2013), and is observationally motivated. However, one needs to keep in mind that an observationally motivated visibility function is effectively averaged over all angles and magnetic fields. More careful analysis requires knowing the fraction of total energy losses that goes into radio emission. Unfortunately, an accurate model of radio emission has yet to be discovered. However, that magnetic fields get factored out will remain true for any visibility function that has the form $V = V_{P,\chi,\xi} V_B$, which allows for a wide range of possible functions.

On the other hand, these considerations do not take into account the pulsar death line. The death line depends on pulsar parameters P, χ and B in a way that does not allow us to factor out the magnetic field birth function. While the death line is not important for the alignment model (Gullón et al. 2014), it is very important for the counter-alignment model (Beskin et al. 1993). The reason is that it acts mostly on pulsars with large inclination angles. In the MHD model, such pulsars are young and energetic and, thus, are not affected by the death line. In the BGI model, the situation is the opposite. This is the reason why we cannot consistently investigate DP interpulses in the BGI model within the approach under consideration.

4.4 Number of interpulse pulsars

We are now in a position to calculate the fraction of pulsars that have interpulse emission. Using solutions (62) and (63), and (66) and (67), visibility functions (25) and (27), as well as normalization (equation 58), we obtain the number of SP and DP interpulses for a variety of models. The results are collected in Table 3.

For the MHD model, we mostly use $Q_\chi = \sin\chi$, which gives an angular distribution function in agreement with observations. For comparison, we also tried $Q_\chi = 2/\pi$ for $W_0 = 5.8^\circ P^{-1/2}$. One can see that because the solution (62) is divergent at small angles, the number of SP interpulses becomes unreasonably large. The number of DP interpulses is not so sensitive to Q_χ, as was seen from Fig. 6. We can, thus, conclude that observations of pulsars at small inclination angles require a random birth function $Q_\chi = \sin\chi$.

For the BGI model, we use $Q_\chi = 2/\pi$, which also gives a flat angular distribution function at small angles. A random birth function $Q_\chi = \sin\chi$ gives a diminishing distribution function $N(\chi)$ and, thus, a very small number of SP interpulses.

Table 3. Prediction of the number of interpulse pulsars for the MHD and BGI models. For SP interpulses, we use criterion (26) to obtain the lower limit, and relation (28) for the upper limit. For DP interpulses, there is no such uncertainty. For each model, we try window widths W_0, corresponding to the core and conal components of emission, as well as a slightly larger value $W_0 = 7.0^\circ P^{-1/2}$. Unless mentioned in the third column, we use $Q_\chi = \sin\chi$ for the MHD model and $Q_\chi = 2/\pi$ for the BGI model. We can conclude that both evolution models are able to reproduce the observations, although they require different birth functions.

Single-pole interpulses ($0.03\,{\rm s} \le P \le 0.5\,{\rm s}$)		
Observations	4/14	
MHD	1/3	$W_0 = 2.45^\circ P^{-1/2}$
BGI	0.2/0.6	
MHD	6/18	$W_0 = 5.8^\circ P^{-1/2}$
BGI	1/4	
MHD	9/26	$W_0 = 7.0^\circ P^{-1/2}$
BGI	2/5	
MHD	17/50	$W_0 = 10.0^\circ P^{-1/2}$
BGI	4/12	
MHD	19/44	$Q_\chi = 2/\pi$
BGI	0.08/0.5	$Q_\chi = \sin\chi$
Double-pole interpulses ($0.03\,{\rm s} \le P \le 0.5\,{\rm s}$)		
Observations	10/23	
MHD	15	$W_0 = 2.45^\circ P^{-1/2}$
MHD	36	$W_0 = 5.8^\circ P^{-1/2}$
MHD	44	$W_0 = 7.0^\circ P^{-1/2}$
MHD	28	$Q_\chi = 2/\pi$

In addition to different evolution models and different inclination angle birth functions Q_χ, we consider different window widths W_0. The value $W_0 = 2.45^\circ P^{-1/2}$ corresponds to the core component of radio emission (Rankin 1990), while the value $W_0 = 5.8^\circ P^{-1/2}$ describes the conal component (Rankin 1993). The latter value is not very well constrained due to the lack of good statistics, so we use additional value $W_0 = 7.0^\circ P^{-1/2}$ to constrain better the number of interpulses (note that this value does not contradict observations of window widths).

For each window width, we calculate upper and lower limits on the SP interpulse fraction using the definitions from Section 2.5.3. As could easily be shown, the number of such pulsars depends quadratically on the window width. For the MHD model, we get the best agreement with observations for $W_0 = 5.8^\circ P^{-1/2}$ with much worse agreement for other window widths. For the BGI model, we obtain the best agreement for $W_0 = 7.0^\circ P^{-1/2}$, and reasonable agreement for $W_0 = 5.8^\circ P^{-1/2}$.

Thus, we can conclude that both models are able to describe the fraction of SP interpulses, and both of them require the use of a visibility function for the conal component (with the BGI model requiring a slightly larger window width).

Our analysis allows us to estimate the number of DP interpulses only for the MHD model. As a result, we get a fraction of such interpulses in good agreement with observations. We obtain the best agreement for core component visibility function $W_0 = 2.45^\circ P^{-1/2}$. This is not surprising: the fit for the core component of radio

Table 4. Prediction of the number of interpulse pulsars for different radio luminosity models. We use $Q_\chi = \sin\chi$ for the MHD model and $Q_\chi = 2/\pi$ for BGI. One can see that the number of interpulse pulsars depends significantly on the luminosity model. On the other hand, the conclusions of Section 4.4 remain true for all models.

Single-pole interpulses, $W_0 = 5.8^\circ P^{-1/2}$		
Observations	4/14	(α_1, α_2)
MHD	1/6	$(-1.5, 0.5)$
MHD	0.5/3	$(-3, 1)$
MHD	4/13	$(-0.8, 1/3)$
BGI	3/9	$(-1.5, 0.5)$
BGI	5/15	$(-3, 1)$
BGI	2/7	$(-0.8, 1/3)$
Double-pole interpulses, $W_0 = 2.45^\circ P^{-1/2}$		
MHD	18	$(-1.5, 0.5)$
MHD	21	$(-3, 1)$
MHD	16	$(-0.8, 1/3)$
Double-pole interpulses, $W_0 = 5.8^\circ P^{-1/2}$		
Observations	10/23	
MHD	44	$(-1.5, 0.5)$
MHD	51	$(-3, 1)$
MHD	40	$(-0.8, 1/3)$

emission (Rankin 1990; Maciesiak et al. 2012) comes from the observations of DP interpulses (for which one can neglect factor $\sin^{-1}\chi$ in the observed window width).

4.5 Dependence on radio luminosity model

Even though we presented a solution of the kinetic equation (59) only for luminosity visibility function $V^{\rm vis}_{\rm lum} = P^{-1}$, the results could be easily generalized for more sophisticated models. Indeed, any luminosity function of the form $L \propto P^{\alpha_1}\dot{P}^{\alpha_2}$ can be expressed as

$$L \propto P^\kappa f^{\rm lum}_\chi(\chi) f^{\rm lum}_B(B) \tag{71}$$

with model-dependent κ, $f^{\rm lum}_\chi$ and $f^{\rm lum}_B$. For example, the MHD model (44) and (45) has $\kappa = \alpha_1 - \alpha_2$, $f^{\rm lum}_\chi = (1+\sin^2\chi)^{\alpha_2}$ and $f^{\rm lum}_B = B^{2\alpha_2}$, while the BGI model (50) and (51) implies $\kappa = \alpha_1 + \alpha_2/14$, $f^{\rm lum}_\chi = \cos\chi^{2d\alpha_2}$ and $f^{\rm lum}_B = B^{10\alpha_2/7}$.

In Table 4, we present the results for the interpulse fraction for different luminosity models. We parametrize each model with power-law indices α_1 and α_2. The most widely used model (see Section 2.3 for a discussion) is $(\alpha_1, \alpha_2) \sim (-1.5, 0.5)$, which corresponds to a luminosity proportional to a potential drop over the polar cap. For comparison, we also include the model with a constant fraction of radio luminosity in the total pulsar losses $L \propto I_r\Omega\dot{\Omega} \propto P^{-3}\dot{P}$. Finally, we use $(\alpha_1, \alpha_2) \sim (-0.8, 1/3)$ to elaborate the analytical prediction (equation 55). Formally, we can use this luminosity model only for BGI evolution theory. However, we include the results for the MHD model for comparison as well.

We can conclude that the results depend significantly on the luminosity model. However, the conclusions of Section 4.4 remain true for all luminosity models. Again, the uncertainties in both observations and theory prevent us from making an exact evaluation of interpulse numbers. We are able to make only an order of magnitude estimate. We see that for such estimates, we have agreement for all models. However, with the growing number of observations, one will be required to have a good physically motivated luminosity model to obtain better agreement with observations.

5 CONCLUSIONS AND DISCUSSION

Analysing now the results collected in Table 3, one can conclude that both the MHD model with the homogeneous birth function $Q_\chi = 2/\pi$ (equation 62) as well as the BGI model for random birth function $Q_\chi = \sin\chi$ (equation 67) are in clear disagreement with observations. The first model predicts too many SP interpulse pulsars while the second one predicts too few. This result can be easily explained.

One can approximately evaluate the number of SP interpulses as

$$\mathcal{N}^{\rm SP} \sim \mathcal{N}_{\rm tot} W_0^2(P_{\rm med}) N^0_\chi / \langle N_\chi(\chi)\sin\chi\rangle_\chi, \tag{72}$$

where N^0_χ is the characteristic value of the angular distribution function near $\chi = 0$, which we take to be $N_\chi[W_0(P_{\rm med})]$. The denominator $\langle N_\chi(\chi)\sin\chi\rangle_\chi$ corresponds to the average value of the angular distribution function of observed pulsars, which should be of order unity, unless most of the pulsars have small angles (for example, the MHD model with uniform angular birth function), and $P_{\rm med}$ is the characteristic value of the period, which we take to be 0.3 s.

For models in good agreement with observations (namely, the MHD model with $Q_\chi = \sin\chi$ and the BGI model with $Q_\chi = 2/\pi$), the estimate (72) gives

$$\mathcal{N}^{\rm SP}_{\rm MHD} \sim 0.05\mathcal{N}_{\rm tot}, \qquad \mathcal{N}^{\rm SP}_{\rm BGI} \sim 0.01\mathcal{N}_{\rm tot}. \tag{73}$$

However, for the MHD model with $Q_\chi = 2/\pi$, the same estimate gives $\mathcal{N}^{\rm SP}_{\rm MHD} \sim 0.1\mathcal{N}_{\rm tot}$, which is too large. Similarly, the BGI model with $Q_\chi = \sin\chi$ predicts $\mathcal{N}^{\rm SP}_{\rm BGI} \sim 0.002\mathcal{N}_{\rm tot}$, which is too small.

Unfortunately, the precision of our considerations does not allow us to select the preferred model. On the other hand, our results put several constraints on the models. In particular, by selecting the model, one fixes the birth functions for the period range $0.03\,{\rm s} \le P \le 0.5$ s:

(i) The MHD model requires a random angular distribution function $Q_\chi = \sin\chi$. At the same time, this model requires the period birth function to be $Q_P = P^{-\kappa-1} \propto$ const.

(ii) The BGI model requires a uniform angular distribution function $Q_\chi = 2/\pi$. At the same time, this model requires the period birth function to be $Q_P = P^{-\kappa} \propto P$.

Here we assume the simplest luminosity model with $\kappa = -1$. For both models, the initial period distribution is rather broad. Our results are in good agreement with the results of Fuller et al. (2015), who computed initial spin periods of neutron stars that were spun up by internal gravity waves during core-collapse supernovae. On the other hand, a stochastic spin-up of the core will inevitably lead to a random orientation of the angular momentum of the neutron star, and, thus, implies $Q_\chi = \sin\chi$, which is one of the requirements of the MHD model.

In addition to predicting the number of interpulse pulsars, our method allows us to determine the observed period distribution of interpulses. For example, one can easily see from equations (27), (25) and (57) that

$$N^{\rm obs,SP}(P) \sim W_0^2(P) N^{\rm obs}(P) \propto P^{-1/2} \tag{74}$$

and

$$N^{\rm obs,DP}(P) \sim W_0(P) N^{\rm obs}(P) \propto {\rm const}. \tag{75}$$

Of course, the current number of observed interpulses is too small to compare their period distribution with our predictions. However, with the growing number of observed interpulses, this will soon become possible.

Finally, as one can see from Table 3, for SP interpulses, the agreement with observations gets better with increasing window width. For DP interpulses, the situation is the opposite. This implies that the emission from low-inclination pulsars is dominated by the conal component, while the emission from high-inclination pulsars is mostly from the core component.

To summarize, one can conclude that the observational data agree with both evolutionary scenarios. The alignment MHD model predicts a reasonable number of both SP and DP interpulse pulsars. For the counter-alignment BGI model, the analytical kinetic approach discussed above can give a suitable number for SP interpulse pulsars only. To analyse DP interpulse pulsars, it is necessary to include:

(i) the death line depending on the magnetic field distribution of neutron stars (see Fig. 3)

(ii) the uncertainty in the antisymmetric current i_a^A, which describes the escape rate for an orthogonal rotator through the death line

(iii) the inclination angle χ dependence of the radio luminosity $L^{\rm BGI}$ (equation 55) resulting in the diminishing of the radio for orthogonal rotators.

We are going to consider this case in a separate paper.

ACKNOWLEDGEMENTS

We thank A. V. Biryukov, Ya. N. Istomin, I. F. Malov, E. B. Nikitina, A. Philippov, J. Pons and S .B. Popov for their interest and useful discussions. This work was partially supported by the Russian Foundation for Basic Research (grant 14-02-00831).

REFERENCES

Arzamasskiy L., Philippov A., Tchekhovskoy A., 2015, MNRAS, 453, 3540
Bagchi M., 2013, Int. J. Modern Phys. D, 22, 1330021
Bai X.-N., Spitkovsky A., 2010, ApJ, 715, 1282
Bates S. D., Lorimer D. R., Rane A., Swiggum J., 2014, MNRAS, 439, 2893
Beskin V. S., Eliseeva S. A., 2005, Astron. Lett., 31, 263
Beskin V. S., Gurevich A. V., Istomin I. N., 1984, Ap&SS, 102, 301
Beskin V. S., Gurevich A. V., Istomin Y. N., 1993, Physics of the Pulsar Magnetosphere. Cambridge Univ. Press, Cambridge
Beskin V. S., Istomin Y. N., Philippov A. A., 2013, Phys. Uspekhi, 56, 164
Davis L., Goldstein M., 1970, ApJ, 159
Faucher-Giguère C.-A., Kaspi V. M., 2006, ApJ, 643, 332
Fuller J., Cantiello M., Lecoanet D., Quataert E., 2015, ApJ, 810, 101
Goldreich P., 1970, ApJ, 160, L11
Good M. L., Ng K. K., 1985, ApJ, 299, 706
Gullón M., Miralles J. A., Viganò D., Pons J. A., 2014, MNRAS, 443, 1891
Lyne A. G., Graham-Smith F., 1998, Cambridge Astrophys. Series, 31, Cambridge Univ. Press, Cambridge
Lyne A. G., Manchester R. N., Taylor J. H., 1985, MNRAS, 213, 613
Lyne A., Graham-Smith F., Weltevrede P., Jordan C., Stappers B., Bassa C., Kramer M., 2013, Science, 342, 598
Maciesiak K., Gil J., Ribeiro V. A. R. M., 2011, MNRAS, 414, 1314
Maciesiak K., Gil J., Melikidze G., 2012, MNRAS, 424, 1762
Malov I. F., Nikitina E. B., 2013, Astron. Rep., 57, 833
Manchester R. N., Taylor J. H., 1977, Pulsars W.H. Freeman and Company, San Francisco
Manchester R. N., Hobbs G. B., Teoh A., Hobbs M., 2005, AJ, 129, 1993
Mestel L., Panagi P., Shibata S., 1999, MNRAS, 309, 388
Philippov A., Tchekhovskoy A., Li J. G., 2014, MNRAS, 441, 1879
Philippov A. A., Spitkovsky A., Cerutti B., 2015, ApJ, 801, L19
Popov S. B., Prokhorov M. E., 2007, Phys. Uspekhi, 50, 1123
Popov S. B., Turolla R., 2012, Ap&SS, 341, 457
Rankin J. M., 1990, ApJ, 352, 247
Rankin J. M., 1993, ApJ, 405, 285
Ruderman M. A., Sutherland P. G., 1975, ApJ, 196, 51
Smith F. G., 1977, Pulsars. Cambridge Univ. Press, Cambridge
Spitkovsky A., 2006, ApJ, 648, L51
Tauris T. M., Manchester R. N., 1998, MNRAS, 298, 625
Tchekhovskoy A., Philippov A., Spitkovsky A., 2016, MNRAS, 457, 3384
Timokhin A. N., Arons J., 2013, MNRAS, 429, 20
Vivekanand M., Narayan R., 1981, JA&A, 2, 315
Weltevrede P., Johnston S., 2008, MNRAS, 387, 1755
Young M. D. T., Chan L. S., Burman R. R., Blair D. G., 2010, MNRAS, 402, 1317
Zanazzi J. J., Lai D., 2015, MNRAS, 451, 695

This paper has been typeset from a TEX/LATEX file prepared by the author.